The International Archives of the Photogrammetry, Remote Sensing and Spatial Information Sciences, Volume XLVIII-1/W6-2025
3rd International Workshop on Evaluation and BENCHmarking of Sensors, Systems and
GEOspatial Data in Photogrammetry and Remote Sensing (GEOBENCH), 20–21 November 2025, Wroclaw, Poland

Adaptable Siemens Star Targets for Reliable and Standardized Spatial Resolution Measurement under DIN 18740-8

Henry Meißner[1,2], Ralf Berger[1]

[1] Institute of Space Research, German Aerospace Center, 12489 Berlin, Germany - (henry.meissner, ralf.berger)@dlr.de
[2] Ostbayerische Technische Hochschule Amberg-Weiden, 92224 Amberg, Germany - h.meissner@oth-aw.de

Keywords: Spatial Resolution, Test Chart, Siemens Star, Image Quality Assessment, Optical Remote Sensing

Abstract

Precise, standardized assessment of spatial resolution is essential for optical remote sensing. We present an adaptable Siemens-star methodology aligned with DIN 18740-8 that enables reliable, reproducible modulation transfer function (MTF) measurements across simulation, laboratory, and aerial (UAV) scenarios. The target geometry is parameterized by star frequency and ground sampling distance (GSD), providing a simple sizing rule for practical deployment. Design variants include multiple segment counts (8–48 Hz) and four gray-level contrasts to mitigate overexposure, a frequent field issue that biases MTF. A phase-based center-detection algorithm — applicable to square- and sinusoidal-type stars — ensures robust centering, a prerequisite for valid MTF estimation. Results show highly consistent MTFs across all configurations: average deviations of 0.007, 0.006, and 0.011 line/pixel for simulation, DSLR, and UAV data, respectively. Center localization exhibits an average two-dimensional error of 0.074 pixels over twenty target variants, confirming numerical stability and implementation accuracy. The scalable vector graphics (SVG) design ensures pixel-exact reproducibility and straightforward scaling to different GSDs while offering practical advantages in production cost, transport, and deployment. Overall, the approach establishes Siemens-star targets as a cost-effective and field-ready alternative to conventional methods, providing standardized procedures, robustness to non-ideal imaging conditions, and direct applicability to both RGB and monochrome systems in operational photogrammetry and remote sensing.
SVG-designs of all Siemens stars as well as the "Resolving-Power" tool to perform the measurments can be downloaded from https://macs.dlr.de/box/resolvingpower.html.

1. Introduction

Spatial resolution is one of the most critical parameters in remote sensing, as it defines the smallest discernible object in an image and directly influences the accuracy of subsequent analyses (Hassani et al., 2023, Liu et al., 2020). Higher spatial resolution enables more precise mapping, improved classification accuracy, and the reliable detection of fine structures, which is essential for applications ranging from environmental monitoring to urban planning. Conversely, insufficient resolution can obscure key spatial patterns and lead to significant errors in interpretation and quantitative assessments.

The determination of spatial resolution is a fundamental task in assessing the quality of imaging systems (Meißner et al., 2017). Among the established methods, the Siemens star has proven to be a robust alternative to the slanted-edge approach, the latter being particularly prone to systematic errors when image sharpening or other post-processing steps are applied (Masaoka et al., 2010, Viallefont-Robinet et al., 2018, Meißner, 2020). A distinctive strength of the Siemens star lies in its adaptability: the effective size of the target is defined by the number of black and white segments, which allows flexible scaling for different sensor characteristics and imaging setups. This flexibility is of particular importance for research groups, scientific institutions, and national mapping agencies, many of which cannot feasibly employ very large test targets (e.g., larger than 3×3 meters) due to cost and logistical constraints.

In practical applications, the reliability of spatial resolution measurements is frequently affected by uncontrolled or variable imaging conditions. One particularly critical factor is the exposure time, which in many imaging systems cannot be freely configured or is automatically adjusted to values that are excessively high. Such conditions often lead to overexposed Siemens-star images, in which bright regions become saturated and fine intensity transitions are lost. This saturation effect significantly alters the measured intensity distribution across the pattern, resulting in distorted modulation transfer function (MTF) estimations and, consequently, a reduced validity of the spatial resolution measurement (see Figure 1).

To ensure reliable and comparable MTF results, it is therefore essential to control exposure parameters as accurately as possible or to implement correction procedures that compensate for saturation effects in the captured imagery.

The work presented in this paper addresses these challenges in three steps.

First, the process of spatial resolution determination using a Siemens star is recapitulated, with emphasis on the mathematical derivation of the required target size.

Second, the influence of design variations is systematically investigated, including changes in the number of black and white segments as well as the introduction of intermediate gray-level intensities. These modifications are evaluated in terms of their effect on the robustness of the measurement and their capacity to mitigate artifacts caused by overexposure.

Third, the applicability of the approach across different imaging modalities is discussed, showing its validity for both RGB and monochrome camera systems, while highlighting its particular suitability for optical remote sensing instruments.

Importantly, the methodology aligns with the current standardization efforts in the field and forms part of the norm

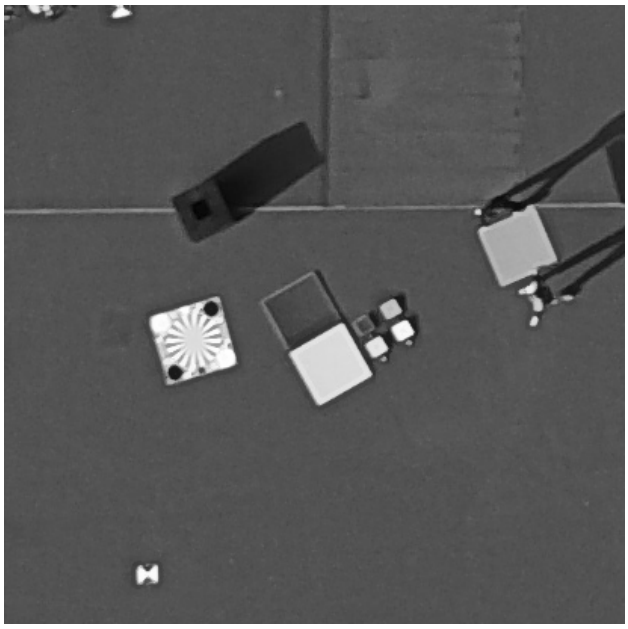

Figure 1. Overexposed drone image.

DIN 18740-8 ”Photogrammetric products – Part 8: Requirements for image quality (quality of optical remote sensing data)”. This ensures not only scientific rigor but also practical relevance for operational frameworks where standardized and reproducible image quality assessment is required (Ghassoun et al., 2021).

This ensures not only scientific rigor but also practical relevance for operational frameworks where standardized and reproducible image quality assessment is required.

The results presented here demonstrate that through careful adjustment of Siemens star design parameters, reliable spatial resolution measurements can be achieved even under non-ideal imaging conditions, thereby providing a scalable and cost-effective solution for a wide range of photogrammetric and remote sensing applications.

The paper provides a comprehensive proof that independently of the target design all spatial resolution measurements and the according center position determination is identical (in justified limits).

2. Mathematical Background

2.1 Size of the Star

To determine the appropriate radius of the Siemens star for spatial resolution measurements, the following formula is applied:

$$r = \frac{3 \cdot s \cdot x}{2 \cdot \pi} + 0.1 \cdot \left(\frac{3 \cdot s \cdot x}{2 \cdot \pi} \right) \tag{1}$$

where s denotes the number of star segments (for example, $s = 16$ for a Siemens star with 8 black and 8 white segments), and x represents the ground sampling distance (GSD). The GSD is derived from the imaging geometry, specifically the focal length of the camera, the flight altitude, and the sensor pixel size. The additional 10% term in the equation accounts for a margin ensuring that the Siemens star fully covers the necessary spatial frequencies without truncation — that is, at least one complete black and white cycle remains visible at the outermost measurable radius (see Figure 2).

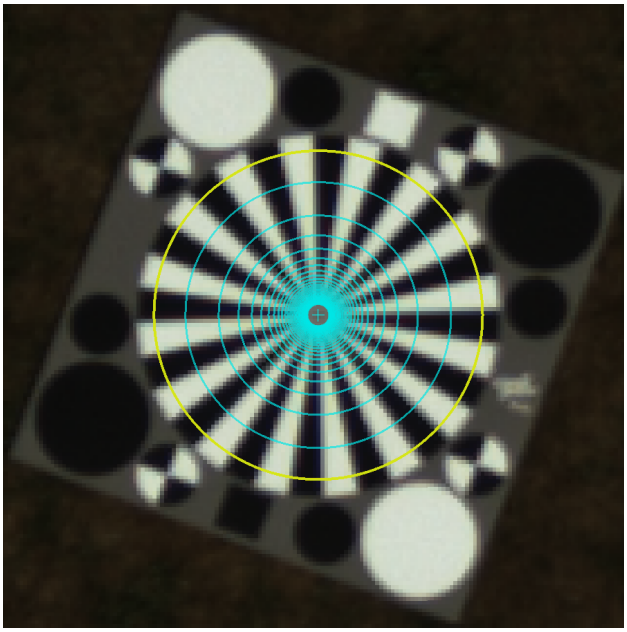

Figure 2. Siemens star including concentric measurement circles to scan intensities.

Equation 1 directly links the physical size of the Siemens star to both the target frequency (number of black–white segment pairs) and the effective GSD of the imaging setup. This relationship allows users to dynamically scale the target size according to the expected resolution of their sensor. For instance, a system with a fine GSD (e.g., an drone camera with small pixel pitch and/or low flight altitude) requires a proportionally smaller target to sample the same spatial frequencies as a coarser GSD system. Conversely, larger GSD values — as encountered in satellite or high-altitude airborne imaging — necessitate a physically larger Siemens star to adequately represent the same frequency content in the image domain.

The factor $\frac{3 \cdot s}{2 \cdot \pi}$ arises from the requirement that three complete pixels be available for reliable MTF estimation. Empirically, this has proven to be a suitable compromise between spatial frequency coverage and manageable target size. The additional margin of 10% serves as a safety factor, ensuring that the outermost measurement circle, used to derive the highest spatial frequency component, remains unaffected by edge truncation or aliasing effects introduced by the image/star boundary.

In practical terms, Equation 1 allows the Siemens star to be tailored to specific imaging scenarios without compromising standardization. When combined with knowledge of the sensor characteristics and flight geometry, the designer can predefine the target diameter to guarantee that the pattern covers the full spatial frequency range up to the system’s Nyquist limit. For operational photogrammetry and remote sensing missions, this adaptability is particularly beneficial: a smaller star can be used for close-range or laboratory measurements, whereas a scaled-up version can be deployed for field calibration or airborne validation campaigns.

To illustrate this, a typical aerial mapping configuration with a

ground sampling distance of 20cm can be considered, as commonly used by federal and national mapping agencies. Applying Equation 1 to a Siemens star with a frequency of 32 Hz (i.e., 64 segments) yields:

$$r = \frac{3 \cdot 32 \cdot 0.20}{2 \cdot \pi} + 0.1 \cdot \left(\frac{3 \cdot 32 \cdot 0.20}{2 \cdot \pi} \right) \approx 6.72\,\mathrm{m} \quad (2)$$

corresponding to a diameter of 13.44m.

This example demonstrates that for high-altitude or medium-resolution applications, even moderate star frequencies quickly result in very large physical targets, underlining the logistical challenges of full-scale deployment. Consequently, scalable and adaptable designs are essential to reduce production cost and effort while maintaining compliance with standardized spatial-resolution requirements.

It is important to note that the relationship between radius, frequency, and GSD also defines the frequency-domain sampling density of the Siemens star. A higher number of segments s increases the angular resolution of the pattern, providing a denser sampling of spatial frequencies, but simultaneously reduces the radial distance between adjacent transitions. Therefore, in practical implementations, the chosen value of s represents a balance between measurement granularity and the physical limitations of printing, optical blur, and camera resolution.

2.2 Spatial Resolution Determination

The underlying theory for spatial resolution determination can be summarized as follows:

The coordinate axis X for contrast transfer function (CTF) and MTF is the spatial frequency k (equation 3) and is calculated as the target frequency k_s divided by the current scan radius r multiplied by π. Siemens star frequency k_s is constant and equivalent to the number of black-white segments.

$$k = \frac{k_s}{\pi r} \quad (3)$$

Related (initially discrete) values for contrast transfer function $C_d\,(k)$ are derived using intensity maxima I_{max} and minima I_{min} for every scanned circle (equation 4). Simultaneously the function value is normalized to contrast level C_0 at spatial frequency equal to 0 (infinite radius).

$$C_d\,(k) = \frac{I_{max}\,(k) - I_{min}\,(k)}{I_{max}\,(k) + I_{min}\,(k)} * \frac{1}{C_0} \quad (4)$$

Continuous function values C are derived by fitting a Gaussian function into discrete input data (equation 5).

$$C = \frac{1}{\sigma\sqrt{2\pi}} e^{-\frac{1}{2}\left(\frac{x-\mu}{\sigma}\right)^2} \quad (5)$$

According to Coltman (Coltman, 1954) the obtained CTF describes the system response to a square wave input while MTF is the system response to a sine wave input. The proposed solution is a normalization with $\frac{\pi}{4}$ followed by series expansion using odd frequency multiples (equation 6).

$$\tilde{H}\,(k) = \frac{\pi}{4} \left[C\,(f) + \frac{C\,(3f)}{3} - \frac{C\,(5f)}{5} + \ldots \right] \quad (6)$$

MTF describes the effective resolving power in frequency domain while PSF $H(r)$ is the image domain equivalent. For this reason both functions are linked directly by fourier transform (equation 7).

$$H(r) \quad \circ\!\!-\!\!\bullet \quad \tilde{H}\,(k) \quad (7)$$

Similar Fourier / polar-domain formulations for Siemens-star–based MTF estimation have been demonstrated for high-resolution imaging systems (Otón et al., 2015).

The described sequence and the implemented algorithm,are already part of the standard "DIN 18740-8 Photogrammetric products – Part 8: Requirements for image quality (quality of optical remote sensing data)".

2.3 Center Determination

There are several ways to determine the star center (Meißner, 2020). One is to use external markers (e.g. rotor shaped marker) included in the design and placed in a way that the intersection of derived line segments deliver the center position (see Figure 2). A further way is to use an image processing step such as detecting lines at the transitions from black to white segments and then calculating all possible intersections and using the average position as Siemens star center. Lastly, the most accurate way is to use a type of phase-correlation. The algorithm can be summarized as follows.

Birch and Griffin analyzed how misalignment of a Siemens-star's center affects MTF determination (Birch and Griffin, 2015). Their approach, developed for sinusoidal Siemens-stars, estimates the offset between the assumed and true center by fitting the scanned intensity profile to a sine function and solving for the horizontal and vertical offsets. However, this method performs poorly on square-wave patterns.

The method used is designed to handle both sinusoidal and square Siemens-stars.

The process begins by identifying the dominant frequency — the sine component with the highest magnitude after a Fourier transform of the outermost circle (low spatial frequency region). The inverse Fourier transform of this dominant component reconstructs a sinusoidal signal approximating the original square wave. Since a spatial shift alters the signal's phase, the phase difference between this reconstructed sine and the measured signal indicates the centering error.

To quantify this shift, peak detection identifies intensity minima and maxima for both signals, comparing their angular positions. Extrema are validated via sign changes in the slope, and the algorithm is applied for all angular positions along each circle. Robustness can be improved by considering a local neighborhood (e.g., ±3 pixels) and discarding weak extrema below a set amplitude threshold.

Peak detection becomes ambiguous for ideal square waves because slopes near extrema are flat, violating certain conditions. This issue is mitigated by exploiting the observation that, as

modulation contrast decreases (below 1), square signals appear more sinusoidal (Figure 4.13). Hence, phase-shift computation is restricted to regions where the modulation contrast $\tilde{H}(k)$ lies between defined bounds, e.g. $b_l = 0.2 < \tilde{H}(k) < b_u = 0.9$ The total phase shift $S(x, y)$ at a given position is obtained by summing the phase differences over all valid extrema and circles between the bounds b_l and b_u. Starting from an initial center estimate (e.g., user-defined), the method evaluates $S(x, y)$ across a small subpixel grid (e.g., ±3 pixels in x and y and a 0.1 pixel step-size). The true center corresponds to the position yielding the minimum cumulative phase shift.

While gradient descent can accelerate this minimization, it risks converging to local minima. Therefore, for standardized and reliable MTF assessment, accuracy and robustness are prioritized over computational speed and a brute force method to scan the entire neighbourhood is used.

3. Experiment Setup

To address the problem of different star designs a simulated test pattern has been developed and evaluated. Figure 5 (at the end of this document) presents a set of Siemens star test targets designed with systematic variations in two key parameters: the number of black and white segments (increasing from top to bottom) and the contrast between dark and bright areas (changing from left to right).

The hypothesis that needs to be proven is that all variations do not affect the effective spatial frequency of the target and thusly do not affect the outcome of resolution measurements. By comparing stars with different segment densities, one can assess the sensitivity of the method to target size and scaling. Similarly, introducing intermediate gray-level intensities instead of pure black-and-white segments allows investigation of how reduced contrast impacts the robustness of modulation transfer function (MTF) estimation, especially under conditions of overexposure or suboptimal illumination.

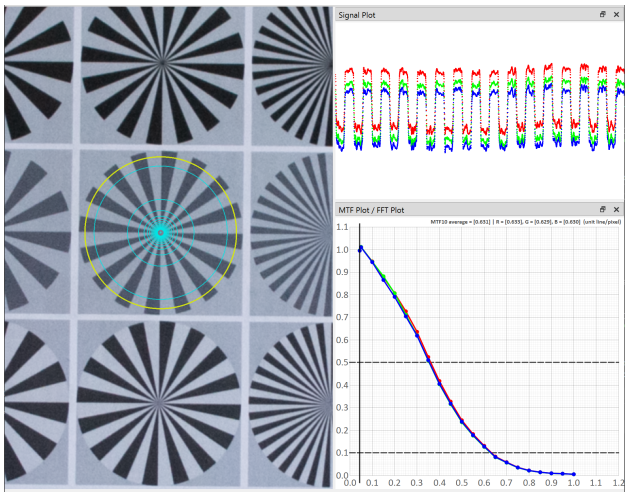

Figure 3. Image of the Siemens star test targets taken with a DSLR (left) example measurement (right).

The experiment procedure is three fold. First, all variations of the Siemens star test targets, differing in both the number of segments and the applied gray-level intensities, were evaluated in a controlled simulation environment. This setup ensured that measurement conditions remained consistent and reproducible, thereby allowing a systematic analysis of how the different design parameters influence the outcome of the spatial resolution assessment. The simulated pattern is a rendered image of all variations and an additive Gaussian blur to simulate real-world spatial resolution. Without this Gaussian blur the image would only yield a pixel MTF which is basically close to a diffraction-limited MTF and totally different from modulation transfer functions of real optical remote sensing systems (Meißner et al., 2019). The Gaussian blur has been implemented as a convolution of the entire image with a two dimensional convolution kernel of three by three pixels simulating a two dimensional Gaussian bell at a sigma of 0.75. Size of the convolution kernel is hereby crucial. With larger kernels a Gaussian bell can be approximated more precisely but when convolving (blurring) pixels of the Siemens star close to the sensor Nyquist-frequency then all pixels of the neighbourhood are used to calculate the new pattern during this pixel-wise operation. For convolution kernel of size five by five or even seven by seven pixels, this means that other segments of the Siemens star are included in the pixel-wise calculation inducing a pattern that may falsify the measurement as it is dependent on the number of Siemens star segments. This circumstance should be considered when aiming to re-establish the experiment.

The second part of the experiment used controlled light conditions of a laboratory but real images of the print-out design have been taken. A digital single-lens reflex (DSLR) camera was used (Sony alpha 7 with a Sony FE 35mm F1.8 lens). The raw images (digital negatives, DNG-format) have been converted to tif-images using Adobe Camera Raw Suite (version 17.8). Subsequently an image showing the various Siemens stars in the center has been chosen and every single configuration was measured (see Figure 3).

The last stage of the experiment is using a drone image to verify the design under real-world operating conditions. The drone used for the experiment was a low-cost off the shelf product but with the capability to take not only compressed jpg imagery but also raw data (digital negatives, DNG-format). Using the same procedure mentioned at stage two of the experiment, Adobe Camera Raw Suite (version 17.8) was used to unpack the raw images to tif-format. Finally, an image showing the design almost centred was chosen to perform all neccessary measurments (see Figure 4).

One of the key prerequisites for accurate spatial resolution assessment is precise determination of the Siemens-star center (see Section 2.3). To evaluate the reliability of the proposed center detection method, the images used for constructing the overall test layout were analyzed. Each individual image was rendered from a scalable vector graphics (SVG) source file, in which the geometric center was defined identically for all twenty design variants. These variants covered spatial frequencies of 8 Hz, 12 Hz, 16 Hz, 32 Hz, and 48 Hz, each combined with four different contrast levels.

The use of an SVG design guarantees pixel-exact reproducibility of geometric features across all image instances, since vector graphics are resolution-independent and mathematically defined. Consequently, the true center position is known a priori and remains consistent among all test patterns. This provides a reliable ground truth for assessing the accuracy and robustness of the implemented center detection algorithm in this study.

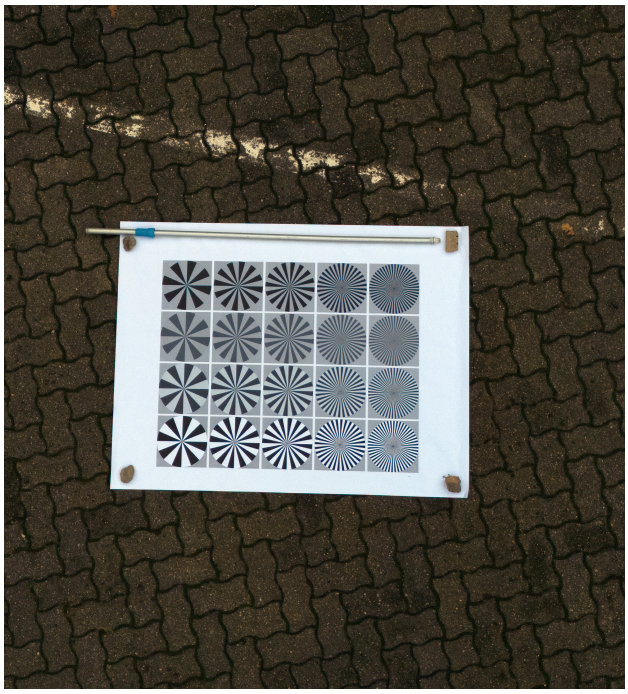

Figure 4. Image of the Siemens star test targets under operating conditions.

4. Results

The following section presents the results obtained from the three-stage experimental procedure described in Section 3. Each stage was designed to successively increase the level of realism — starting from a fully controlled simulation environment, progressing to laboratory measurements under stable illumination, and finally extending to real-world aerial imagery. This stepwise approach enables a systematic evaluation of the proposed method's robustness against variations in imaging conditions and optical system characteristics.

4.1 Simulation Results

Intensity	**Frequency [Hz]**				
High_Low [%]	8 Hz	12 Hz	16 Hz	32 Hz	48 Hz
066_000	0.569	0.558	0.555	0.551	0.550
065_035	0.553	0.543	0.541	0.539	0.536
080_020	0.561	0.548	0.546	0.544	0.542
100_000	0.571	0.557	0.556	0.552	0.549
Mean	**0.564**	**0.552**	**0.550**	**0.547**	**0.544**

Table 1. Measured MTF values at different spatial frequencies and varying intensities for the simulated test pattern.

In the first stage, all Siemens-star design variations were evaluated under simulated conditions to establish a baseline for the measurement accuracy and reproducibility of the implemented approach. The rendered test patterns allowed a controlled examination of how the number of segments and gray-level intensity settings influence the measured modulation transfer function (MTF). The resulting MTF values for the investigated configurations at selected spatial frequencies are summarized in Table 1. The results show that all measurements exhibit remarkably similar MTF responses across the tested variations. The average deviation of 0.007 [line / pixel] confirms the high stability and reproducibility of the method.

4.2 Laboratory Results

Intensity	**Frequency [Hz]**				
High_Low [%]	8 Hz	12 Hz	16 Hz	32 Hz	48 Hz
066_000	0.613	0.625	0.618	0.621	0.618
065_035	0.626	0.624	0.632	0.618	0.611
080_020	0.630	0.631	0.624	0.621	0.620
100_000	0.617	0.616	0.625	0.634	0.634
Mean	**0.622**	**0.624**	**0.625**	**0.624**	**0.621**

Table 2. Measured MTF values at different spatial frequencies and varying intensities for the test pattern imaged with a DSLR.

The resulting MTF values obtained from the DSLR measurements are summarized in Table 2. Similar to the simulation results, all evaluated Siemens-star configurations show consistent MTF characteristics across the tested spatial frequencies. The average deviation of only 0.006 [line per pixel] demonstrates a high level of measurement stability and reproducibility under real imaging conditions. This small variation confirms that the printed test targets and the implemented evaluation algorithm remain robust with respect to changes in contrast and segment frequency.

Minor differences between configurations can primarily be attributed to optical imperfections, illumination inhomogeneities and sensor noise which are expected in practical setups. Overall, the results validate that the Siemens-star design performs reliably when captured with a DSLR camera under controlled laboratory conditions.

4.3 Aerial (Drone) Results

Intensity	**Frequency [Hz]**				
High_Low [%]	8 Hz	12 Hz	16 Hz	32 Hz	48 Hz
066_000	0.607	0.570	0.588	0.579	0.572
065_035	0.623	0.570	0.599	0.571	0.572
080_020	0.577	0.589	0.581	0.575	0.579
100_000	0.569	0.565	0.565	0.569	0.564
Mean	**0.594**	**0.574**	**0.583**	**0.574**	**0.572**

Table 3. Measured MTF values at different spatial frequencies and varying intensities for the drone imagery.

The results obtained from the drone imagery are summarized in Table 3. Compared to the simulation and DSLR measurements, the MTF values exhibit slightly higher variability, which reflects the more demanding imaging conditions during aerial data acquisition. The average deviation of 0.011 [line per pixel] nevertheless confirms the overall stability and reliability of the applied method, even under uncontrolled outdoor conditions.

Across all tested configurations, the measured values remain within a narrow range, indicating that the Siemens-star design preserves its diagnostic sensitivity despite changes in altitude,

https://doi.org/10.5194/isprs-archives-XLVIII-1-W6-2025-139-2025

Intensity	8 Hz		12 Hz		16 Hz		32 Hz		48 Hz	
High_Low [%]	x	y	x	y	x	y	x	y	x	y
066_000	2083.48	2083.53	2083.51	2083.34	2083.43	2083.38	2083.48	2083.47	2083.50	2083.52
065_035	2083.53	2083.54	2083.40	2083.34	2083.47	2083.58	2083.48	2083.48	2083.51	2083.51
080_020	2083.44	2083.53	2083.40	2083.37	2083.48	2083.57	2083.44	2083.48	2083.53	2083.49
100_000	2083.48	2083.52	2083.42	2083.37	2083.47	2083.58	2083.52	2083.47	2083.49	2083.47
Mean	**2083.48**	**2083.53**	**2083.43**	**2083.36**	**2083.46**	**2083.53**	**2083.48**	**2083.48**	**2083.51**	**2083.50**

Table 4. Siemens star center location measurements of all variations (x and y values). Average 2D-deviation is 0.074 pixels.

illumination, and atmospheric influence. Minor fluctuations between individual measurements can be attributed to motion-induced blur, radiometric inhomogeneities, or small deviations in sensor focus.

Overall, the findings demonstrate that the proposed workflow is sufficiently robust for practical application in airborne imaging scenarios, providing consistent and interpretable MTF results from real-world data.

4.4 Center Determination Results

The results of the center detection evaluation are summarized in Table 4. The measured center coordinates for all Siemens-star configurations show only very minor deviations from the expected position. The average two-dimensional distance of 0.074 pixels between the detected centers and the mean reference position clearly demonstrates the high precision and robustness of the implemented algorithm. This extremely small deviation, which is well below the pixel level, confirms that the procedure reliably identifies the geometric center even across variations in spatial frequency and contrast.

The consistent results across all twenty test patterns also validate the stability of the measurement process and the numerical accuracy of the implementation. No systematic displacement or directional bias could be observed, indicating that the algorithm performs symmetrically in both x- and y-directions. These findings strongly support the validity of the proposed approach for precise center localization — a prerequisite for reliable MTF analysis based on Siemens-star targets.

5. Conclusion and Outlook

The given paper demonstrated that adaptable Siemens-star targets enable reliable and standardized spatial-resolution measurements across a wide range of imaging conditions and target designs, consistent with DIN 18740-8. In controlled simulations, laboratory DSLR data, and aerial imagery, the measured MTF curves remained highly consistent across variations in segment frequency and gray-level contrast. The average deviations between configurations were 0.007, 0.006, and 0.011 line/pixel for simulation, DSLR, and drone data, respectively, indicating strong robustness from idealized to operational scenarios. Accurate center localization — critical for Siemens-star analysis — showed an average 2D error of 0.074 pixels, confirming both the measurement stability and the numerical reliability of the implementation. Together, these results establish that users can tune target frequency and contrast to practical constraints (e.g. size and exposure management) without compromising the validity of MTF estimation.

Beyond accuracy, the study highlights practical advantages of the proposed approach: (i) vector-based designs ensure pixel-exact reproducibility and straightforward scaling to different GSDs; (ii) contrast variants mitigate saturation or overexposure effects common in field acquisition; and (iii) the center-detection strategy functions reliably for all Siemens star variations. These properties make the targets suitable for RGB and monochrome systems and for deployments where large physical charts are impractical. In addition, the findings demonstrate that significant design flexibility can be achieved without sacrificing accuracy, allowing the Siemens-star target to be reduced in size and production cost while maintaining full analytical validity. This flexibility greatly simplifies transport, deployment, and reuse in laboratory and outdoor settings, thus lowering the overall effort required for standardized spatial-resolution testing.

Future work will benchmark against slanted-edge and other standardized methods to quantify agreement and complementarity and provide an open, reference implementation with standard operating procedures and quality flags to support broader adoption and the ongoing standardization under DIN 18740-8.

References

Birch, G. C., Griffin, J. C., 2015. Sinusoidal Siemens star spatial frequency response measurement errors due to misidentified target centers. *Optical Engineering*, 54(7), 074104–074104.

Coltman, J. W., 1954. The specification of imaging properties by response to a sine wave input. *JOSA*, 44(6), 468–471.

Ghassoun, Y., Gerke, M., Khedar, Y., Backhaus, J., Bobbe, M., Meissner, H., Tiwary, P. K., Heyen, R., 2021. Implementation and validation of a high accuracy UAV-photogrammetry based rail track inspection system. *Remote Sensing*, 13(3), 384.

Hassani, K., Gholizadeh, H., Taghvaeian, S., Natalie, V., Carpenter, J., Jacob, J., 2023. Assessing the impact of spatial resolution of UAS-based remote sensing and spectral resolution of proximal sensing on crop nitrogen retrieval accuracy. *International Journal of Remote Sensing*, 44(14), 4441–4464.

Liu, M., Yu, T., Gu, X., Sun, Z., Yang, J., Zhang, Z., Mi, X., Cao, W., Li, J., 2020. The impact of spatial resolution on the classification of vegetation types in highly fragmented planting areas based on unmanned aerial vehicle hyperspectral images. *Remote Sensing*, 12(1), 146.

Masaoka, K., Sugawara, M., Nojiri, Y., 2010. Multidirectional mtf measurement of digital image acquisition devices using a siemens star. *Digital Photography VI*, 7537, SPIE, 295–302.

Meißner, H., 2020. *Determination and improvement of spatial resolution obtained by optical remote sensing systems*. Humboldt University Berlin (Germany).

Meißner, H., Cramer, M., Piltz, B., 2017. Benchmarking the optical resolving power of UAV based camera systems. *The International Archives of the Photogrammetry, Remote Sensing and Spatial Information Sciences*, 42, 243–249.

Meißner, H., Cramer, M., Reulke, R., 2019. Evaluation of structures and methods for resolution determination of remote sensing sensors. *Pacific-Rim Symposium on Image and Video Technology*, Springer, 59–69.

Otón, J., Sorzano, C. O. S., Marabini, R., Pereiro, E., Carazo, J. M., 2015. Measurement of the modulation transfer function of an X-ray microscope based on multiple Fourier orders analysis of a Siemens star. *Optics express*, 23(8), 9567–9572.

Viallefont-Robinet, F., Helder, D., Fraisse, R., Newbury, A., van den Bergh, F., Lee, D., Saunier, S., 2018. Comparison of MTF measurements using edge method: towards reference data set. *Optics express*, 26(26), 33625–33648.

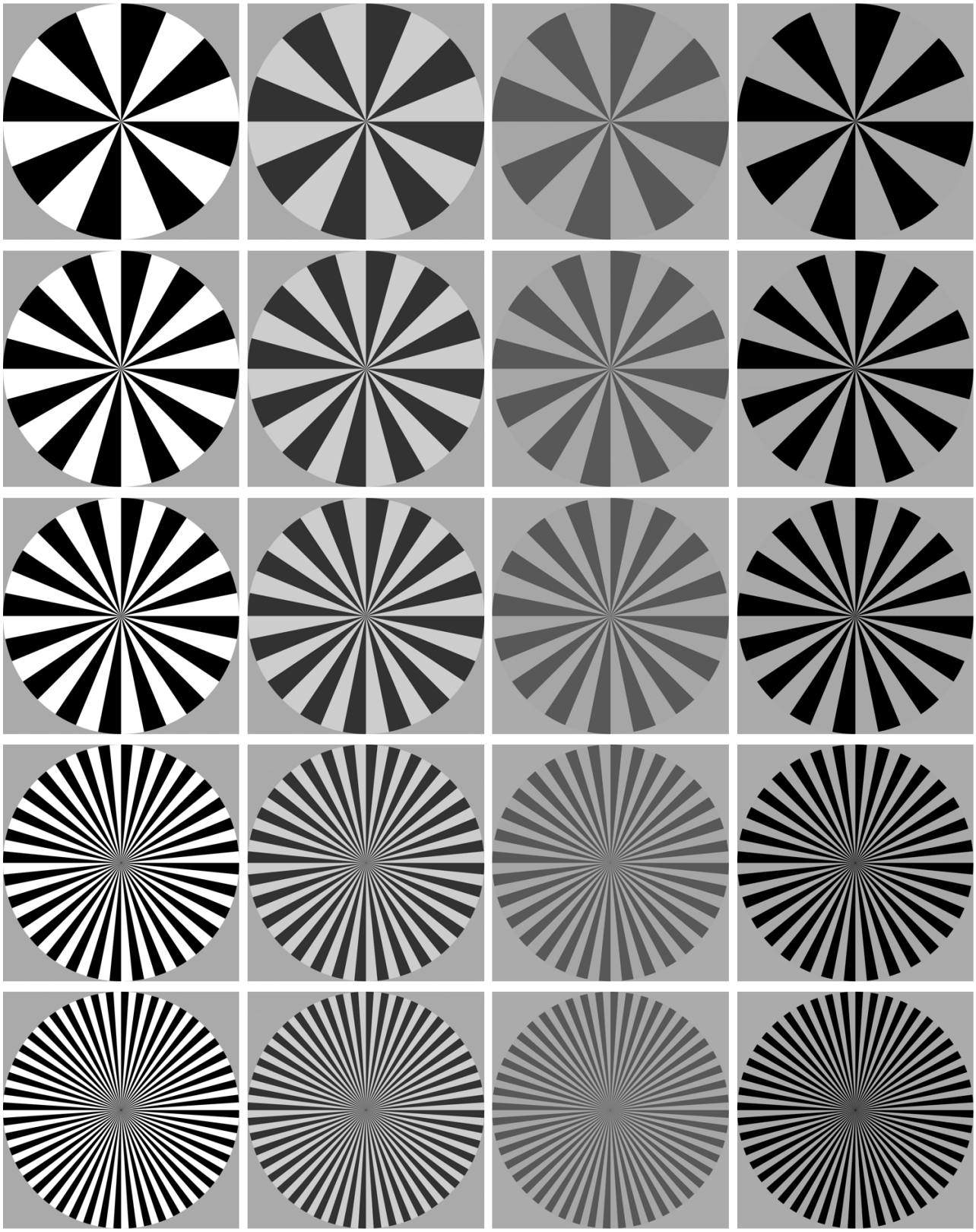

Figure 5. Siemens star test targets with varying numbers of segments (top to bottom) and gray-level intensities (left to right).

https://doi.org/10.5194/isprs-archives-XLVIII-1-W6-2025-139-2025